



Simple approach for electronic structure calculations on self-organized perovskite quantum dot filmsC. I. Cabrera ^{*}*Unidad Académica de Ciencia y Tecnología de la Luz y la Materia, Universidad Autónoma de Zacatecas,
98160 Zacatecas, Zacatecas, Mexico**and Centro de Investigación en Ciencias, Instituto de Investigación en Ciencias Básicas y Aplicadas,
Universidad Autónoma del Estado de Morelos, 62209, Cuernavaca, Morelos, Mexico*R. Pérez-Álvarez [†]*Centro de Investigación en Ciencias, Instituto de Investigación en Ciencias Básicas y Aplicadas,
Universidad Autónoma del Estado de Morelos, 62209, Cuernavaca, Morelos, Mexico*

(Received 10 April 2023; accepted 12 July 2023; published 25 July 2023)

All-inorganic perovskite quantum dots films have received significant research interest for photovoltaic applications because of their better mechanical durability than bulk film and the various tunable properties that perovskite quantum dots exhibit. Here we develop a simple, almost analytic approach to calculating the electronic states in self-organized perovskite quantum dot systems. We present an extension to the tight-binding method, where the role of atoms is now played by quantum dots. This generalized tight-binding approach is applied to assess the feasibility of achieving miniband formation through phenyl-C₆₀-butyric acid methyl ester (PCBM)/CsPbI₃ quantum dots films. Type-II band alignment in these hybrid heterostructures led to the development of a nearly-free-electron model combined with a Hartree variational approach for describing conduction-band states. By implementing our approach, we reveal that PCBM/CsPbI₃ quantum dot films are indirect-band-gap systems. A 41-meV bandwidth for the hole ground miniband is found due to the coupling between dots. Energy-gap values consistent with the experiment are obtained. This approach opens the way for calculating relevant optical properties in a broad class of perovskite quantum dot systems, such as the absorption coefficient.

DOI: [10.1103/PhysRevB.108.035147](https://doi.org/10.1103/PhysRevB.108.035147)**I. INTRODUCTION**

Perovskite solar cells are one the most promising emerging technologies in the field of photovoltaics, with certified power conversion efficiencies (PCEs) above 25% [1]. Colloidal perovskite quantum dots (PQDs) have various superior properties over bulk perovskites, such as efficient multiexciton effects, size-dependent optical and electronic states, extraordinary defect tolerance, and high-quality quantum dot (QD) film deposited at room temperature [2–5]. Currently, all-inorganic CsPbI₃ QD is highly desired for solar-harvesting technologies, because this composition can withstand temperatures of more than 460 °C [6,7], and surface strain enables QDs to remain in the perovskite phase at room temperature [4,8,9]. Moreover, CsPbI₃ QD solar cells achieved a PCE of more than 16%, exceeding that of traditional PbS QDs, showing great potential for efficient flexible photovoltaics [9–11].

In general, the approach to form arrays of close-packed PQDs is to spin coat and/or heat treat colloidal solutions of QDs developing the formation of a self-organized QD film [11,12]. Thus the quantum-mechanical coupling between QDs increases with decreasing interdot distance, and the confined levels overlap to form minibands [13,14]. The miniband for-

mation is expected in either perfect or disordered QD arrays with small interdot distances [15]. The QDs in these disordered arrays only exhibit local order due to a size distribution of about 10% [7]. Therefore, to achieve a significant formation of delocalized, extended states, it is important to improve the size distribution of QDs.

The standard approaches to the energy-band structure of QD arrays are the finite-element method and the Kronig-Penney model within an effective-mass envelope-function framework [13,16–18]. However, the simplicity of this approximation comes at a cost that includes the following: (i) phenomena associated with the Bloch functions of carriers that are symmetrized to the lattice system are neglected. (ii) There are regions outside the dots where the potential is overestimated by assuming it as the sum of three independent periodic functions in orthogonal directions. Thus the coupling among neighboring dots decreases, which leads to an underestimation of the miniband widths.

Here we develop a simple, almost analytic, alternative approach for the band structure of perovskite QD systems, where the Bloch states are considered. Furthermore, the potential outside the dots is not overestimated, avoiding a decrease in the coupling of wave functions between neighboring dots. The system being examined is an organic compound/CsPbI₃ QD hybrid film. The organic molecule phenyl-C₆₀-butyric acid methyl ester (PCBM) is introduced into the CsPbI₃ QD layers, forming a hybrid heterojunction in which holes

^{*}carlos.cabreraperdomo@uaz.edu.mx[†]rpa@uaem.mx

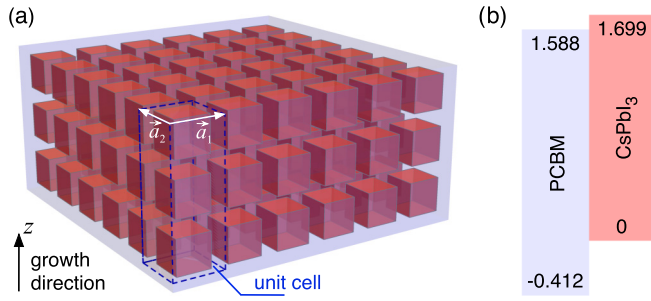


FIG. 1. (a) Schematic representation of the perovskite quantum dot system modeled as an array of regularly spaced, equal-sized cubic dots on a square periodic lattice in an organic material matrix. The system has a finite number of quantum dot layers in the growth direction. The dashed blue line defines a unitary cell. (b) Type-II band alignment for PCBM/CsPbI₃ hybrid heterostructure with hole confinement at perovskite dots [20].

are confined in the PQDs and electrons move almost freely through the organic matrix, see Fig. 1. Assuming the dots are the same size and aligned, which makes sense at least locally, as schematically illustrated in Fig. 1(a), the formation of the hole minibands is to be expected in this system. Nevertheless, the generality of our approach makes it suitable for studying the band structure of a variety of coupled quantum dot systems in a relatively simple and computationally fast way.

In this paper we introduce a simple approach to assess the feasibility of achieving miniband formation through PCBM/CsPbI₃ quantum dots films. We present an extension to the tight-binding (TB) method originally suggested by Bloch [19], by considering QDs instead of atoms, in order to calculate the valence-band (VB) states. For the description of conduction-band (CB) states, we develop a nearly-free-electron model combined with a Hartree variational approach that allows capturing the effects of finite film thickness on the band structure. We describe the electronic-band-gap dependence on the QD layer number for PQD films. The predicted energy band gap for PCBM/CsPbI₃ quantum dot films is consistent with experimental data.

II. DESCRIPTION OF THE APPROACH

For QD films, we are only interested in the valence- and conduction-band structure, which describe the system's fundamental optical and electronic properties. In this work we assumed that the states near the band edges behave very much like the ground states they had when they were isolated.

The valence-band states of the system are formed from localized states in the perovskite quantum dots, while the conduction-band states come from delocalized electronic states at the matrix material. For this reason we use different electronic band-structure calculation methods for valence and conduction bands. The first method consists of a tight-binding approach, and the second one utilizes a Hartree variational approach to calculate the VB and CB states, respectively. The appeal of these methods is that the electronic structure can be calculated by solving a one-electron Schrödinger wave equation which is computationally less expensive than

ab initio calculations and provides a relatively easy means of generating the electronic band structure.

First, we start by finding the ground-state energy in isolated quantum dots that constitute the system. We implemented a variational method based on using a Gaussian trial wave function in the form

$$\phi_0(\vec{r}) = A e^{-\alpha r^2/2}, \quad (1)$$

where A is a normalization constant, $r = |\mathbf{r}|$, and the parameter α is adjusted in order to minimize the expectation value of the Hamiltonian operator,

$$\hat{H} = -\frac{\hbar^2}{2m(\mathbf{r})} \nabla^2 + v_{QD}(\mathbf{r}), \quad (2)$$

with $m(\mathbf{r})$ and $v_{QD}(\mathbf{r})$ depicting the position-dependent electron effective mass and the confinement potential which is labeled by V_D^v and V_M^v within the dot and matrix region, respectively.

A. Valence-band states of the system: Tight-binding approach

For the present approach, as shown in Fig. 1, the system's structure is described in terms of the geometry of the arrangement of identical quantum dots in the unit cell. The positions of QDs in the unit cell are described by the vector $\boldsymbol{\tau}_s$ and the array of unit cells remaining unchanged by the translation,

$$\mathbf{R}_\mathbf{u} = u_1 \mathbf{a}_1 + u_2 \mathbf{a}_2, \quad (3)$$

where the subscript \mathbf{u} indicates a collection of two integers u_1 , u_2 and \mathbf{a}_1 , \mathbf{a}_2 that are mutually orthogonal primitive translation vectors with $|\mathbf{a}_1| = |\mathbf{a}_2| = a$.

In our TB approach, where the role of atoms is assumed by quantum dots, the eigenstates of the QDs in the unit cell of a given QDs system are used as the basic expansion set for the Bloch function of the array. Let $\phi_{\mu s}(\mathbf{r} - \mathbf{r}_{\mathbf{u}s})$ indicate the eigenstate defined by quantum numbers μ ($\mu = 0, 1, \dots$, with $\mu = 0$ indicating the ground state) for a QD located in position $\boldsymbol{\tau}_s$ ($s = 0, 1, \dots$, with $s = 0$ labeling the QD at the bottom of the unit cell) in the unit cell $\mathbf{R}_\mathbf{u}$. It is convenient to define, for any eigenstate $\phi_{\mu s}(\mathbf{r} - \mathbf{r}_{\mathbf{u}s})$, the corresponding Bloch sum $\Phi_{\mu s}(\mathbf{k}, \mathbf{r})$ of vector \mathbf{k} ,

$$\Phi_{\mu s}(\mathbf{k}, \mathbf{r}) = \frac{1}{\sqrt{N}} \sum_{\mathbf{u}} e^{i\mathbf{k} \cdot \mathbf{R}_\mathbf{u}} \phi_{\mu s}(\mathbf{r} - \mathbf{r}_{\mathbf{u}s}), \quad (4)$$

where $\mathbf{r}_{\mathbf{u}s} = \mathbf{R}_\mathbf{u} + \boldsymbol{\tau}_s$, and N is the number of unit cells in the system.

The Hamiltonian of the QD system is given in the form

$$\hat{H}^v = \hat{T} + \sum_{\mathbf{u}} \sum_s V_{\mathbf{u}s}(\mathbf{r}), \quad (5)$$

where \hat{T} is the kinetic energy operator, and the second term on the right-hand side of Eq. (5) describes the QD system potential where $V_{\mathbf{u}s}(\mathbf{r}) = V_0(\mathbf{r} - \mathbf{r}_{\mathbf{u}s})$ represents the QD-like potential for a QD located in position $\boldsymbol{\tau}_s$ in the unit cell $\mathbf{R}_\mathbf{u}$. We next consider the matrix elements of the Hamiltonian, $H_{\mu's';\mu s}^v = \langle \Phi_{\mu's'}(\mathbf{k}, \mathbf{r}) | H^v | \Phi_{\mu s}(\mathbf{k}, \mathbf{r}) \rangle$, which are given by

$$H_{\mu's';\mu s}^v = \sum_{\mathbf{u}} e^{i\mathbf{k} \cdot \mathbf{R}_\mathbf{u}} (E_{\mu's'} S_{\mu's';\mu s}^{0;\mathbf{u}} + v_{\mu's';\mu s}^{0;\mathbf{u}}), \quad (6)$$

where $E_{\mu's'}$ is the energy of the μ' -th eigenstate for an isolated QD in position $\mathbf{r}_{s'}$ in the unit cell, $S_{\mu's';\mu s}^{0;\mathbf{u}} = \langle \phi_{\mu's'}(\mathbf{r} - \mathbf{r}_{0s'}) | \phi_{\mu s}(\mathbf{r} - \mathbf{r}_{\mathbf{u}s}) \rangle$ denotes the overlap integral between two QD eigenstates, and $v_{\mu's';\mu s}^{0;\mathbf{u}} = \langle \phi_{\mu's'}(\mathbf{r} - \mathbf{r}_{0s'}) | v_{\mathbf{u}s}(\mathbf{r}) | \phi_{\mu s}(\mathbf{r} - \mathbf{r}_{\mathbf{u}s}) \rangle$ is the potential integral with $v_{\mathbf{u}s}(\mathbf{r}) = \sum_{\mathbf{u}} \sum_s V_{\mathbf{u}s}(\mathbf{r}) - V_{\mathbf{u}s'}(\mathbf{r})$ as the difference between the potential of the QD system and the potential of the QD located in $\mathbf{r}_{\mathbf{u}s'}$.

The localized states of QDs decay rapidly away from the QD, and it is expected that the overlap integral $S_{\mu's';\mu s}^{0;\mathbf{u}} \approx 0$, for large $\mathbf{R}_{\mathbf{u}}$. Therefore we only include the overlap and potential integrals between nearest-neighbor QDs in our calculation.

The potential integral in Eq. (6) is split into two parts, within each of which the potential is constant,

$$v_{\mu's';\mu s}^{0;\mathbf{u}} = V_D^v D_{\mu's';\mu s}^{0;\mathbf{u}} + V_M^v M_{\mu's';\mu s}^{0;\mathbf{u}}, \quad (7)$$

where the overlap integral $D_{\mu's';\mu s}^{0;\mathbf{u}}$ is taken over the dots region with constant average potential V_D^v , and $M_{\mu's';\mu s}^{0;\mathbf{u}}$ is taken over the matrix region with constant average potential V_M^v . For simplicity, we take the energy to be zero at the valence-band edge of bulk perovskite, i.e., the bottom of QDs, $V_D^v = 0$, as shown in Fig. 1(b). Then, substituting Eq. (7) into Eq. (6), we finally arrive at the expression for the Hamiltonian matrix elements,

$$H_{\mu's';\mu s}^v = \sum_{\mathbf{u} \in \eta} e^{i\mathbf{k} \cdot \mathbf{R}_{\mathbf{u}}} (E_{\mu's'} S_{\mu's';\mu s}^{0;\mathbf{u}} + V_M^v M_{\mu's';\mu s}^{0;\mathbf{u}}), \quad (8)$$

where η represents the collection of two integers that generates the translation vectors to the nearest neighbor QDs.

In our tight-binding approach, the eigenstates of the QD system are the zeros of the secular determinant [21]:

$$\det(\langle \Phi_{\mu's'} | \hat{H}^v - E | \Phi_{\mu s} \rangle) = 0. \quad (9)$$

In the case of a layer of QDs, the system contains a QD per unit cell, which leads to a unique Bloch sum $\Phi_{\mu s}(\mathbf{k}, \mathbf{r})$ if only one state is considered per QD. Then we obtain the following expression for the corresponding eigenstates of the one-layer system of QDs:

$$E(\mathbf{k}) = E_{\mu s} + V_M^v \frac{\sum_{\mathbf{u} \in \eta} e^{i\mathbf{k} \cdot \mathbf{R}_{\mathbf{u}}} M_{\mu s; \mu s}^{0;\mathbf{u}}}{\sum_{\mathbf{u} \in \eta} e^{i\mathbf{k} \cdot \mathbf{R}_{\mathbf{u}}} S_{\mu s; \mu s}^{0;\mathbf{u}}}. \quad (10)$$

For the overlap integral $M_{\mu's';\mu s}^{0;\mathbf{u}}$, a similar expression is obtained but integrated over the matrix region.

B. Conduction-band states of the system: Hartree approximation

Conduction electrons can move almost freely in the matrix region through the QD array. So we can treat the QD system's potential, $V_{QD}(\mathbf{r})$, as a periodic potential added to the Hamiltonian of a free electron. The total Hamiltonian describing the system has the form

$$\hat{H}^c = \hat{T}_1 + \hat{T}_2 + V_{QD}(\mathbf{r}), \quad (11)$$

where $\hat{T}_1 = -\frac{\hbar^2}{2m^*} \nabla_{\rho}^2$ and $\hat{T}_2 = -\frac{\hbar^2}{2m^*} \nabla_z^2$ are the kinetic energy operators expressed in terms of the in-plane and out-of-plane coordinates ρ and z , respectively and $m^* = 0.84m_0$ is the electron effective mass in bulk PCBM [22] with m_0 denoting

the free-electron mass. We define $V_{QD}(\mathbf{r})$ as

$$V_{QD}(\mathbf{r}) = V_1(\rho) + U(\rho, z), \quad (12)$$

where $V_1(\rho)$ represents the potential of a square cross-section quantum wire system with cross-section S_D of area c^2 , where c is the side length of the PQD. Furthermore, the quantum wire system is invariant under translations given by Eq. (3). Here $U(\rho, z) = [V_M^c - V_1(\rho)]f(z)$, V_M^c denotes the conduction-band edge of the matrix material, and $f(z)$ is given by the expression

$$f(z) = 1 - \sum_{i=1}^{N_l} \Theta(z - l_i) \Theta(r_i - z), \quad (13)$$

where $l_i = (i-1)(c+d) - W/2$ and $r_i = l_i + c$ are the left and right boundary positions for the i th QD layer, respectively, and $W = cN_l + d(N_l - 1)$ is the QD film thickness. Θ represents the Heaviside step function, N_l denotes the number of QD layer in the film, and d labels the interdot distance. The function $f(z)$ plays an important role in modeling the QD system's potential. In the z intervals where $f(z)$ is equal to 1, the potential $V_1(\rho)$ is replaced by the potential V_M^c , leading to a layered system of QDs from a quantum wire system.

In the Hartree approximation, we assume that the eigenstates of the total Hamiltonian $\Psi(\vec{r})$ can be written as a product of states dependent on ρ and z coordinates in the form

$$\Psi(\mathbf{r}) = \varphi_1(\rho) \varphi_2(z). \quad (14)$$

Let us define the quantity

$$K(\varphi_1, \varphi_2) = \langle \Psi | \hat{H}^c | \Psi \rangle - \sum_{i=1}^2 \epsilon_i \langle \varphi_i | \varphi_i \rangle, \quad (15)$$

where the Lagrange multipliers ϵ_i associated with the normalization condition of the φ_i have been introduced. For $\Psi(\mathbf{r})$ to be a solution of the Hamiltonian \hat{H}^c , the functional derivative of $K(\varphi_1, \varphi_2)$ with respect to the functions φ_1 and φ_2 must be stationary. As a result, we obtain the following system of coupled integro-differential equations for the φ_i states:

$$[\hat{T}_1 + V_1'(\rho) - \epsilon_1'] \varphi_1(\rho) = 0, \quad (16)$$

$$\left[\hat{T}_2 + f(z) \Delta V^c N \int_{S_D} ds |\varphi_1(\rho)|^2 - \epsilon_2 \right] \varphi_2(z) = 0. \quad (17)$$

Here

$$V_1'(\rho) = V_1(\rho) \left[1 - \int_{-\infty}^{\infty} dz \varphi_2^*(z) f(z) \varphi_2(z) \right], \quad (18)$$

$$\epsilon_1' = \epsilon_1 - V_M^c \int_{-\infty}^{\infty} dz \varphi_2^*(z) f(z) \varphi_2(z), \quad (19)$$

and $\Delta V^c = V_M^c - V_D^c$, with V_D^c denoting the conduction-band edge of the dot material and N is the number of unit cells in the QD film. Equation (17) describes a one-dimensional problem of a layered system in which the number of barriers corresponds to the number of QD layer in the film. Otherwise, Eq. (16) describes the in-plane motion of a nearly free particle in a quantum wire system with the same two-dimensional lattice as that of the QD film given by Eq. (3) and eigenenergy ϵ_1' . The wave function φ_1 solution of Eq. (16) has the same

periodicity of the lattice and therefore satisfies the normalization condition $N \int_{S_U} ds \varphi_1^*(\boldsymbol{\rho}) \varphi_1(\boldsymbol{\rho}) = 1$, where S_U denote the $\hat{\mathbf{z}}$ cross section of the unit cell. Therefore the integral in Eq. (17) can be bounded in the form

$$0 \leq \gamma = N \int_{S_D} ds |\varphi_1(\boldsymbol{\rho})|^2 \leq N \int_{S_U} ds |\varphi_1(\boldsymbol{\rho})|^2 = 1, \quad (20)$$

where γ denotes the probability of finding an electron in the dot material.

In order to obtain the eigensolution of the set of Eqs. (16) and (17), we first assign an input value $\gamma_{\text{in}} \in [0, 1]$ to γ in Eq. (17), and then we solve the corresponding one-dimensional problem. Once the wave function φ_2 and the corresponding eigenenergy ϵ_2 have been calculated, the next step is to find the in-plane wave function φ_1 and the corresponding eigenenergy ϵ_1 using Eqs. (16) and (19). Finally, we evaluate the output value γ_{out} for γ through its definition given in Eq. (20). If the output value of γ_{out} matches the input value γ_{in} , we have found an eigenstate $\Psi(\mathbf{r})$ and its corresponding eigenenergy $\epsilon = \epsilon_1 + \epsilon_2$ for the QD system. In brief, it is essentially a root-finding procedure for $\gamma_{\text{in}} - \gamma_{\text{out}}$.

To solve the one-dimensional problem described by Eq. (17), the wave function φ_2 was expanded as a linear combination of a basis set, $\{\chi_i(z)\}$, of the solutions of the rectangular quantum well, with infinite barrier height and width \mathcal{L} ; $\varphi_2(z) = \sum_i C_i \chi_i(z)$. The boundary \mathcal{L} is the ‘‘quantum thickness of the film,’’ which represents the length over which the energy levels are well defined and is placed away from the layered system. The Hamiltonian matrix elements are evaluated within the basis set $\{\chi_i(z)\}$, and the resulting Hamiltonian matrix is diagonalized to yield C_i [23]. To solve the Schrödinger equation (16) we use the usual nearly-free-electron approach, where a restatement of the equation in momentum space is given in the form

$$\left[\frac{\hbar^2}{2m^*} |\mathbf{k} - \mathbf{K}_m|^2 - \epsilon_1(\mathbf{k} - \mathbf{K}_m) \right] \beta_{\mathbf{k}-\mathbf{K}_m} + \sum_{\mathbf{n}} \bar{V}_{\mathbf{n}-\mathbf{m}} \beta_{\mathbf{k}-\mathbf{K}_n} = 0, \quad (21)$$

where $\beta_{\mathbf{k}-\mathbf{K}_n}$ are the coefficients of the plane-wave expansion of the wave function φ_1 ,

$$\varphi_{1\mathbf{k}}(\boldsymbol{\rho}) = e^{i\mathbf{k}\cdot\boldsymbol{\rho}} \sum_{\mathbf{n}} \beta_{\mathbf{k}-\mathbf{K}_n} e^{-i\mathbf{K}_n\cdot\boldsymbol{\rho}}, \quad (22)$$

where the sum is over all reciprocal lattice vectors \mathbf{K}_n , and $\bar{V}_{\mathbf{n}}$ represents the Fourier transform of the quantum wire system’s potential $V_1(\boldsymbol{\rho})$, with subscript \mathbf{n} indicating a collection of two integers n_1, n_2 . We arrive at the expression for $\bar{V}_{\mathbf{n}}$:

$$\bar{V}_{\mathbf{n}}(z) = V_M^c \delta_{n_1 0} \delta_{n_2 0} - \Delta V^c g(n_1) g(n_2), \quad (23)$$

where the function $g(n)$ is given in the form

$$g(n) = \begin{cases} \frac{1}{\pi n} \sin(\pi n c/a), & n \neq 0; \\ c/a, & n = 0. \end{cases} \quad (24)$$

Thereby, the band-structure calculation is reduced to solving the eigenvalue problem specified by Eq. (21). For a fixed \mathbf{k} in the first Brillouin zone there is a set of equations in the form (21) for all reciprocal lattice vectors \mathbf{K}_n , and the many

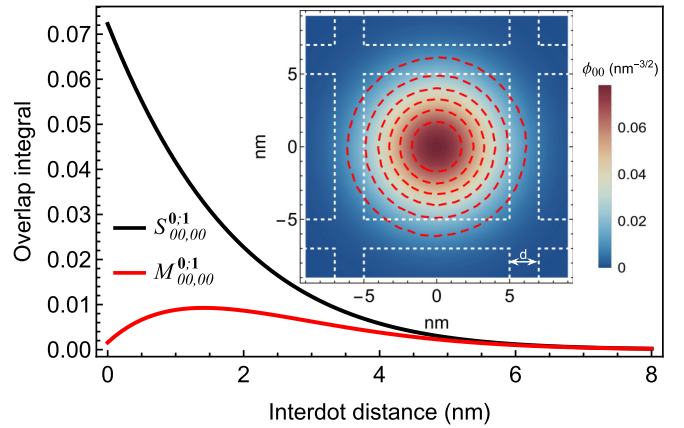


FIG. 2. Overlap integral $S_{00,00}^{0:1}$ and potential integral $M_{00,00}^{0:1}$ in units of the matrix region potential V_M^v between the ground states ϕ_{00} of two nearest-neighbor QDs for a film formed by a QD layer. The inset shows a normalized ground-state horizontal slice of the wave function ϕ_{00} at the center of an isolated cubic dot. A significant exponential decay inside the barrier is also displayed, showing the potential formation of minibands from localized states.

different solutions to (21) for a given \mathbf{k} are labeled with the band index \mathbf{n} . The number of reciprocal lattice vectors used determines both the matrix size and calculation accuracy.

III. IMPLEMENTATION OF THE MODEL: PCBM/CsPbI₃ QD FILMS

We investigated the electronic-band-gap and miniband formation for PCBM/CsPbI₃ quantum dot films. The system is modeled as an array of regularly spaced cubic dots in a fixed-thickness PCBM matrix as shown in Fig. 1(a). The perovskite dot dimensions are described by $c = 10$ nm, and the interdot distance in each coordinate direction is $d = 2$ nm. Here a tight-binding approach is used to calculate the valence-band structure and wave functions, while to compute the conduction-band states, we use a Hartree variational approach. The PCBM forms a type-II band alignment with CsPbI₃ QDs: Holes are confined in dot regions, representing barriers for electrons, see Fig. 1(b). The values of band offset and band gaps of 1.694 eV and 2 eV for CsPbI₃ and PCBM, respectively, were taken from the literature [20]. The parameter values used in our calculations were $V_M^v = -412$ meV [20], $\Delta V^c = 109$ meV [20], as shown in Fig. 1(b). The effective mass of holes in the quantum dot and matrix material are $0.095 m_0$ [24] and $1.65 m_0$ [22], respectively. Experimental values of PQD film thickness are not accurately reported in the literature [11,12,25]. However, our model assumes isolated QD films with a thickness of 200 nm, so \mathcal{L} matches the thickness of the films. Our \mathcal{L} value is a good approximation of the average of the film thicknesses estimated in Refs. [11], [12,25]. Finally, we compared the calculated electronic band gap with the experimental optical gap reported in the three previous papers.

The overlap integrals $S_{\mu'\mathbf{s}';\mu\mathbf{s}}^{0:\mathbf{u}}$ and potential integrals $v_{\mu'\mathbf{s}';\mu\mathbf{s}}^{0:\mathbf{u}}$ between wave functions of neighboring dots were calculated in order to compute the valence-band dispersion relation of the QD system. Figure 2 shows the effect of the

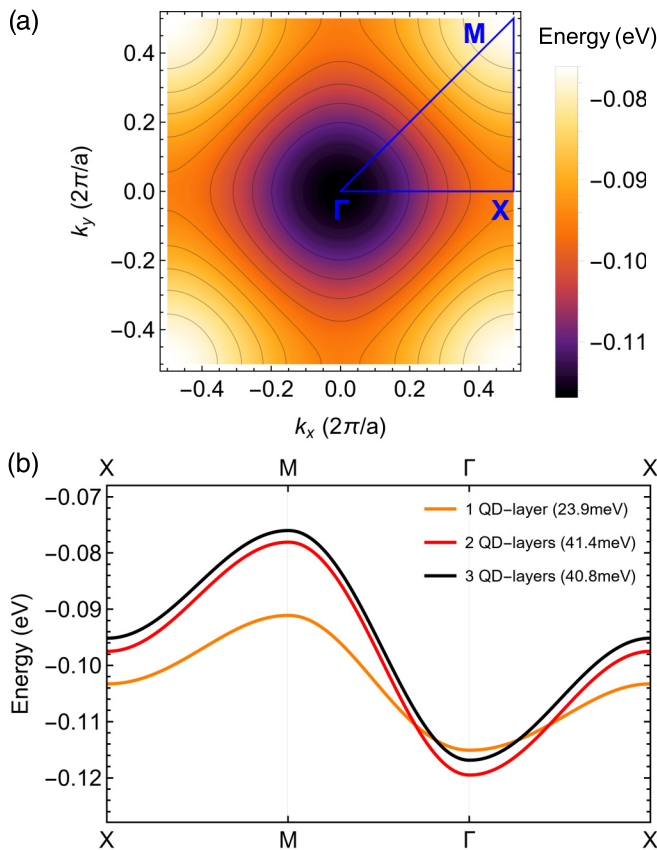


FIG. 3. (a) Contour plot of the miniband energy within the first Brillouin zone for a square two-dimensional lattice of a film based on three QD layers. Only the ground state of perovskite QDs and the interactions up to the second neighbor's coordination sphere were considered in the calculations. Gray lines represent isoenergetic curves. (b) Miniband structure for several films which differs in the number of QD layers. Miniband width values are shown in parentheses.

proximity between nearest-neighboring dots on the overlap between ground-state wave functions and potential integrals, which are calculated for a film formed by a layer of QDs. Notice from Fig. 2 that the potential integral scales with the interdot distance, up to a maximum for 1.4 nm, after which it decreases. By increasing the interdot distance, the potential integral value is increased due to the increased matrix region, but the interaction between dots, which is described through the overlap integral, is reduced and consequently, the potential integral value decreases.

Assuming that only the ground state from each QD contributes to the states of the system, we use Eqs. (9) and (10) to calculate the valence-miniband dispersion relation for several perovskite QD films. Miniband energy contours within the first Brillouin zone for a film formed by three QD layers is shown in Fig. 3(a). Dispersions given along the k line connecting $X - M - \Gamma - X$ for several PQD films in the TB approach are displayed in Fig. 3(b). Miniband width values are shown in parentheses in the figure legend and are taken as the difference between the maximum and minimum allowed miniband energy. Also, note from Fig. 3(b) that the top of the minibands shifts to higher energies with increasing QD

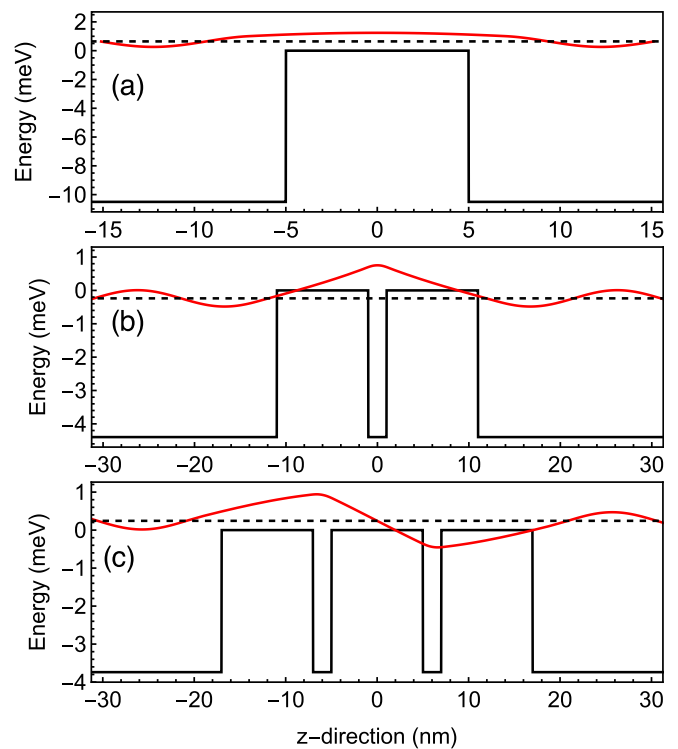


FIG. 4. Effective potential profile and normalized ground-state wave function for electrons in the vicinity of barrier systems. Black dashed line represents the ground energy level calculated for the one-dimensional problem given by Eq. (17). Each barrier corresponds to a layer of perovskite quantum dots: (a) one QD layer, (b) two QD layers, and (c) three QD layers. Here energy zero corresponds to the conduction-band edge of the bulk matrix material.

layers. The presence of the other QDs depresses the potential throughout the system. Furthermore, the increasing number of interactions between neighboring dots leads to a decrease in the carrier effective mass and consequently, an increase in the miniband width. It is worth noting that films with three or more QD layers were all found to have quite similar miniband formations. This is because the overlap integral is significant up to the second neighbor's coordination sphere.

Once the structure of valence bands and the corresponding Bloch states have been described, we proceed to study the conduction-band states of the system. Here we focus on the band edge formed by the conduction-band ground states of the system, so we take the minimum γ value that satisfies the set of Eqs. (16) and (17). Figure 4 displays the normalized ground-state wave function in the vicinity of the barrier system and corresponding eigenenergy ϵ_2 of the one-dimensional problem given by Eq. (17) for several perovskite QD systems. Being isolated QD films, the electrons are restricted to a finite region \mathcal{L} , i.e., infinitely high potential barriers outside this region. The barrier system potential profiles are plotted in the figure as well. To ensure convergence within 0.1 meV for all barrier systems, we use a basis set of 400 wave functions. Notice from Fig. 4 that by increasing the QD layer number the barrier height is reduced and consequently, the probability of finding an electron in the dot material decreases; see the coupling term in Eq. (17) containing an integration over the

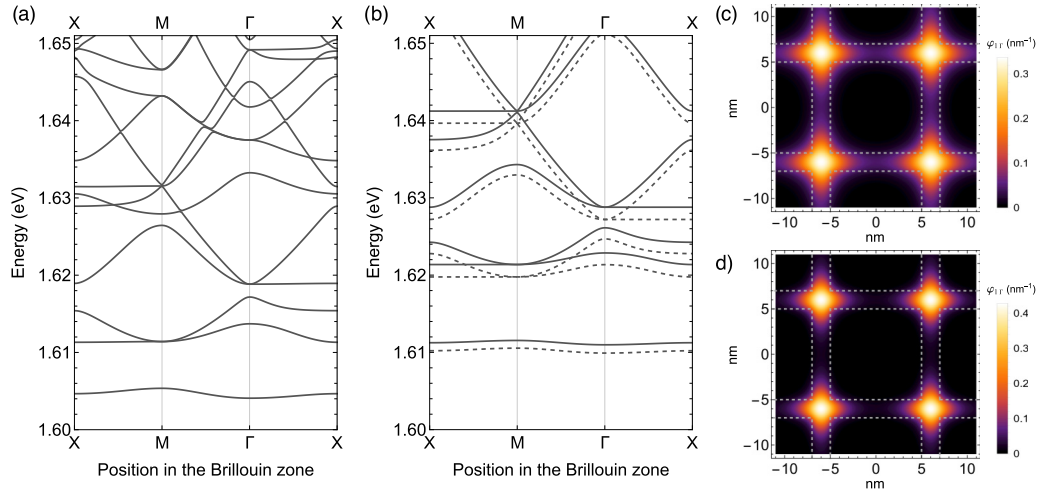


FIG. 5. Calculated conduction-band structure for the in-plane problem described by Eq. (16) for films with one (a), two (b, dashed line), and three (b, solid line) quantum dot layers. Normalized ground-state wave function $\varphi_1(\boldsymbol{\rho})$ at point Γ for the film problem with one (c) and three (d) quantum dot layers. Wave functions are normalized over the unit cell area S_U . Adding quantum dot layers causes a band shift toward high energies and decreases the electron probability density in the dot material.

S_D area. The effect of QD layers addition on the conduction states of the system is mentioned below in the discussion of Fig. 5.

In order to solve the two-dimensional problem described by the eigenvalue equation (21), the Fourier transform of the in-plane effective potential $V_1'(\boldsymbol{\rho})$ was evaluated by means of expression (23). In our calculations, 625 plane waves are sufficient to expand the wave function $\varphi_{1\mathbf{k}}$, expression (22), and the potential $V_1'(\boldsymbol{\rho})$ ensuring convergence within 0.1 meV. Each plane wave corresponds to a vector in the reciprocal lattice, and the expansion should be symmetric about the reciprocal lattice origin to guarantee real eigenvalues. We confirmed that the difference in energy calculated using 625 and 2025 plane waves in the Fourier expansion is less than 0.1 meV, which indicates that convergence is being achieved. This confirmation allows us to reduce the computational efforts of the eigenvalue problem.

By varying the wave vector \mathbf{k} values, both the conduction-band structure and the normalized ground-state wave function $\varphi_1(\boldsymbol{\rho})$ for the in-plane problem (i.e., quantum wires problem), defined according to Eq. (16), are obtained for perovskite quantum dot films (see Fig. 5). Note that a band shift towards high energies occurs due to QD layer incorporation. Specifically, the lower energy miniband experiences a 7-meV increment at point Γ when varying the QD layer number from 1 to 3. Adding more layers causes the energy to increase by less than 1 meV, as shown in Fig. 7(a). Furthermore, with the incorporation of QD layers, the probability of locating electrons in the interstices between quantum wires increases, and the exponential decay distance of the wave function in the quantum wire region decreases, as shown in Figs. 5(c) and 5(d). This behavior occurs as a consequence of an increment in the maximum value of the two-dimensional periodic potential in Eq. (18) together with the above-mentioned decrease in the barrier height in Eq. (17) with QD layer incorporation.

Next, both the wave function $\Psi(\mathbf{r})$ of the system's electron states and the eigenenergies are finally obtained. Figure 6 shows the electron probability density in the vicinity of the

dots, $|\Psi(\mathbf{r})|^2$, at point Γ for PCBM/CsPbI₃ quantum dot films. Adding QD layers causes a ground-state shift to higher energies, allowing electrons to diffuse relatively freely into the matrix material above and below the QD layers. Besides this behavior, it is reasonable to expect that the electrons are somewhat constrained within the interstitial space by the surrounding dots. This behavior can be more pronounced as the number of QD layers increases in fixed-thickness films. A balance between these two phenomena defines the electron density probability for a given film.

We examine the effect of quantum-dot-layer incorporation on the electronic-band-gap values for CsPbI₃ QD films [see Fig. 7(a)]. Theoretical computations suggest that the band gap decreases with QD layer number and eventually remains almost constant, with an increment in energy lower than 1 meV, from three QD layers onwards.

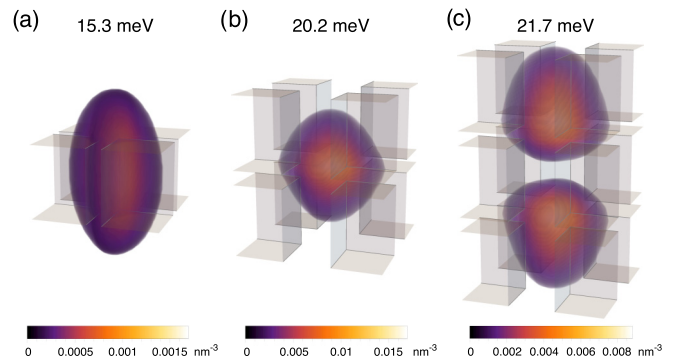


FIG. 6. Calculated electron probability density for CsPbI₃ quantum dot arrays embedded in a PCBM matrix, with cubic dots (in gray) of side length equal to 10 nm and an interdot distance equal to 2 nm. The numbers are the corresponding eigenenergies in meV. The plotted density corresponds to values greater than 0.08 of the maximum wave function square values, respectively. Here, the energy zero corresponds to the conduction-band edge of bulk PCBM material.

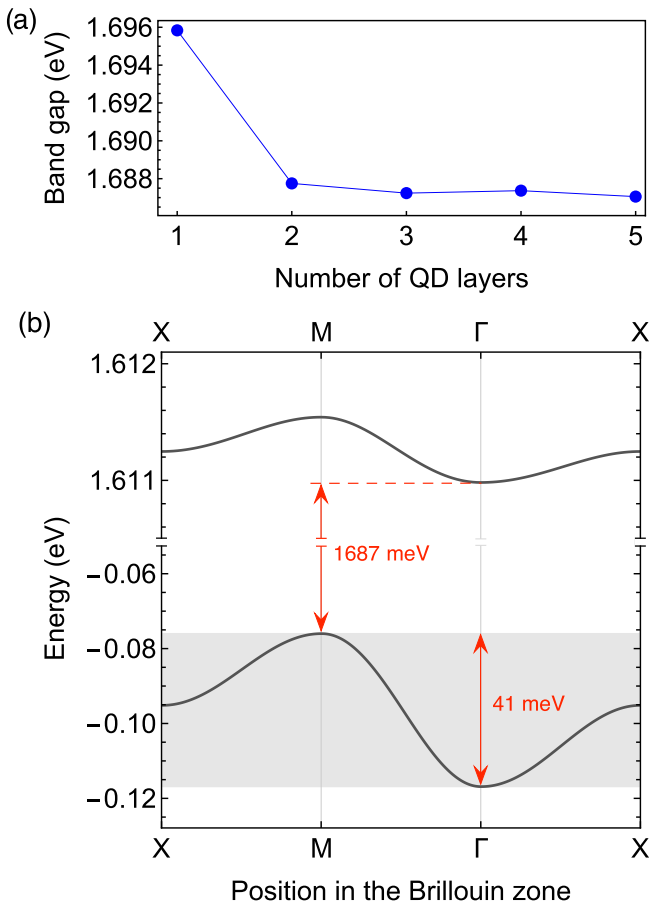


FIG. 7. Electronic band gap dependence with QD layer number for PCBM/CsPbI₃ quantum dot films (a) and calculated band-edge structure (b) of a film composed of three QD layers. The electronic band gap is indicated in the band structure at the M point.

The band-edge dispersion relation obtained for electron and hole states of a PCBM/CsPbI₃ quantum dot film formed by three QD layers is illustrated in Fig. 7(b). A 41-meV bandwidth is revealed for the hole ground miniband due to wave function coupling between neighboring dots in the studied perovskite quantum dot systems. Our calculations show that PCBM/CsPbI₃ quantum dot films are indirect-band-gap systems. Its electronic band gap is calculated from the valence-band maximum at the M point to the conduction-band minimum at the Γ point. The band gap, using the materials parameters and the PCBM/perovskite band offset values mentioned above, is calculated to be $E_g = 1.687$ eV, which is consistent with experimental findings (1.75 eV [11,12,25]). We mainly attribute the discrepancy between the calculated band gap and the experimental value for the optical gap

of PCBM/CsPbI₃ QD films to the omission of both dot size effects and in-plane periodicity breaking in our calculations. The size-dependent tensile strain can have significant effects on the optical and structural properties [7]. These size-dependent effects are understudied and should be further explored; they have not been reported for many PQD systems. Additionally, both size distribution and randomly arranged QDs in a disordered film lead to the coexistence of localized and delocalized states [15]. Thus optical transitions between the discrete and bandlike states of this mixture are possible.

IV. CONCLUSIONS

A simple approach to calculating the electronic states in self-organized perovskite quantum dot systems has been developed and applied to PCBM/CsPbI₃ PQD films. In the framework of the tight-binding method, we assumed quantum dots in the role of atoms and extend the method originally suggested by Bloch to arrays of quantum dots. We found a significant quantum coupling that leads to the formation of energy minibands. The hole miniband width was calculated to be 41 meV for the ground states in the systems considered. We developed a nearly-free-electron model combined with a Hartree variational approach for describing conduction-band states due to a type-II band alignment with hole confinement. By mathematically constructing the potential of the quantum dot system from the potential of a quantum wire system, the solution to the three-dimensional conduction-band problem was simplified to the solution of two coupled lower-dimensional problems. Our approach allows the finite thickness of the films to be considered in band-structure calculations. It was shown that from three QD layers the film can be considered thick for the purposes of its band structure. This is partly because significant coupling interactions between dots occur up to the second neighbor's coordination sphere. By applying our approach, we revealed that PCBM/CsPbI₃ quantum dot films are indirect-band-gap systems. We found consistency between the computed band-gap value of 1.69 eV and the reported experimental value of 1.75 eV deduced from photoluminescence spectra. The simplicity and adaptability of the approach to other QD-based systems, together with its modest computational requirements, make it an ideal tool for analyzing experimental data and a starting point for calculating relevant optical properties.

ACKNOWLEDGMENTS

C.I.C. acknowledges CONACYT for Postdoctoral Research Fellowship I1200/224/2021 and the UAEM for its hospitality. The authors are thankful for the careful review from the referees.

The authors declare no conflict of interest.

[1] O. Almora, D. Baran, G. C. Bazan, C. I. Cabrera, S. Erten-Ela, K. Forberich, F. Guo, J. Hauch, A. W. Y. Ho-Baillie, T. J. Jacobsson, R. A. J. Janssen, T. Kirchartz, N. Kopidakis, M. A. Loi, R. R. Lunt, X. Mathew, M. D. McGehee, J. Min, D. B. Mitzi, M. K. Nazeeruddin *et al.*, Device performance of

emerging photovoltaic materials (version 3), *Adv. Energy Mater.* **13**, 2203313 (2023).

[2] J. Yuan, A. Hazarika, Q. Zhao, X. Ling, T. Moot, W. Ma, and J. M. Luther, Metal halide perovskites in quantum dot solar cells: Progress and prospects, *Joule* **4**, 1160 (2020).

- [3] J. Khan, I. Ullah, and J. Yuan, CsPbI₃ perovskite quantum dot solar cells: Opportunities, progress and challenges, *Mater. Adv.* **3**, 1931 (2022).
- [4] A. Swarnkar, A. R. Marshall, E. M. Sanehira, B. D. Chernomordik, D. T. Moore, J. A. Christians, T. Chakrabarti, and J. M. Luther, Quantum dot-induced phase stabilization of α - CsPbI₃ perovskite for high-efficiency photovoltaics, *Science* **354**, 92 (2016).
- [5] J. Yuan, X. Ling, D. Yang, F. Li, S. Zhou, J. Shi, Y. Qian, J. Hu, Y. Sun, Y. Yang, X. Gao, S. Duhm, Q. Zhang, and W. Ma, Band-aligned polymeric hole transport materials for extremely low energy loss α - CsPbI₃ perovskite nanocrystal solar cells, *Joule* **2**, 2450 (2018).
- [6] R. J. Sutton, G. E. Eperon, L. Miranda, E. S. Parrott, B. A. Kamino, J. B. Patel, M. T. Hörantner, M. B. Johnston, A. A. Haghighirad, D. T. Moore, and H. J. Snaith, Bandgap-tunable cesium lead halide perovskites with high thermal stability for efficient solar cells, *Adv. Energy Mater.* **6**, 1502458 (2016).
- [7] Q. Zhao, A. Hazarika, L. T. Schelhas, J. Liu, E. A. Gaulding, G. Li, M. Zhang, M. F. Toney, P. C. Serce, and J. M. Luther, Size-dependent lattice structure and confinement properties in CsPbI₃ perovskite nanocrystals: Negative surface energy for stabilization, *ACS Energy Lett.* **5**, 238 (2020).
- [8] Q. Zhao, A. Hazarika, X. Chen, S. P. Harvey, B. W. Larson, G. R. Teeter, J. Liu, T. Song, C. Xiao, L. Shaw *et al.*, High efficiency perovskite quantum dot solar cells with charge separating heterostructure, *Nat. Commun.* **10**, 2842 (2019).
- [9] D. Jia, J. Chen, R. Zhuang, Y. Hua, and X. Zhang, Inhibiting lattice distortion of CsPbI₃ perovskite quantum dots for solar cells with efficiency over 16.6%, *Energy Environ. Sci.* **15**, 4201 (2022).
- [10] M. Hao, Y. Bai, S. Zeiske, L. Ren, J. Liu, Y. Yuan, N. Zarrabi, N. Cheng, M. Ghasemi, P. Chen *et al.*, Ligand-assisted cation-exchange engineering for high-efficiency colloidal Cs_{1-x}FA_xPbI₃ quantum dot solar cells with reduced phase segregation, *Nat. Energy* **5**, 79 (2020).
- [11] L. Hu, Q. Zhao, S. Huang, J. Zheng, X. Guan, R. Patterson, J. Kim, L. Shi, C.-H. Lin, Q. Lei *et al.*, Flexible and efficient perovskite quantum dot solar cells via hybrid interfacial architecture, *Nat. Commun.* **12**, 466 (2021).
- [12] F. Li, S. Zhou, J. Yuan, C. Qin, Y. Yang, J. Shi, X. Ling, Y. Li, and W. Ma, Perovskite quantum dot solar cells with 15.6% efficiency and improved stability enabled by an α - CsPbI₃/FAPbI₃ bilayer structure, *ACS Energy Lett.* **4**, 2571 (2019).
- [13] C.-W. Jiang and M. A. Green, Silicon quantum dot superlattices: Modeling of energy bands, densities of states, and mobilities for silicon tandem solar cell applications, *J. Appl. Phys.* **99**, 114902 (2006).
- [14] O. L. Lazarenkova and A. A. Balandin, Miniband formation in a quantum dot crystal, *J. Appl. Phys.* **89**, 5509 (2001).
- [15] B. B. Smith and A. Nozik, Theoretical studies of electronic state localization and wormholes in silicon quantum dot arrays, *Nano Lett.* **1**, 36 (2001).
- [16] D. Eric, J. Jiang, A. Imran, M. N. Zahid, and A. A. Khan, Optical properties of InN/GaN quantum dot superlattice by changing dot size and interdot spacing, *Results Phys.* **13**, 102246 (2019).
- [17] W. Hu, M. F. Budiman, M. Igarashi, M.-Y. Lee, Y. Li, and S. Samukawa, Modeling miniband for realistic silicon nanocrystal array, *Math. Comput. Modell.* **58**, 306 (2013).
- [18] L. M. Pérez, A. E. Aouami, K. Feddi, V. Tasco, A. B. Abdellah, F. Dujardin, M. Courel, J. A. Riquelme, D. Laroze, and E. M. Feddi, Parameters optimization of intermediate band solar cells: Cases of PbTe/CdTe, PbSe/ZnTe and InN/GaN quantum dots, *Crystals* **12**, 1002 (2022).
- [19] F. Bloch, Über die quantenmechanik der elektronen in kristallgittern, *Z. Phys.* **52**, 555 (1929).
- [20] M. K. Hossain, M. H. K. Rubel, G. I. Toki, I. Alam, M. F. Rahman, and H. Bencherif, Effect of various electron and hole transport layers on the performance of CsPbI₃-based perovskite solar cells: A numerical investigation in DFT, SCAPS-1D, and wxAMPS frameworks, *ACS Omega* **7**, 43210 (2022).
- [21] G. F. Bassani and G. Pastori Parravicini, *Electronic States and Optical Transitions in Solids*, 1st ed., edited by R. A. Ballinger (Pergamon Press Oxford, New York, 1975).
- [22] M. B. Salim and R. Nekovei, Designing of PCBM derivative using pyridazine compound for more efficient bulk heterojunction organic solar cell, in *2021 IEEE 48th Photovoltaic Specialists Conference (PVSC)* (IEEE, New York, 2021), pp. 1009–1013.
- [23] J.-B. Xia and W.-J. Fan, Electronic structures of superlattices under in-plane magnetic field, *Phys. Rev. B* **40**, 8508 (1989).
- [24] M. A. Becker, R. Vaxenburg, G. Nedelcu, P. C. Serce, A. Shabaev, M. J. Mehl, J. G. Michopoulos, S. G. Lambrakos, N. Bernstein, J. L. Lyons *et al.*, Bright triplet excitons in caesium lead halide perovskites, *Nature (London)* **553**, 189 (2018).
- [25] K. Chen, W. Jin, Y. Zhang, T. Yang, P. Reiss, Q. Zhong, U. Bach, Q. Li, Y. Wang, H. Zhang *et al.*, High efficiency mesoscopic solar cells using CsPbI₃ perovskite quantum dots enabled by chemical interface engineering, *J. Am. Chem. Soc.* **142**, 3775 (2020).